Proc. Natl. Acad. Sci. USA
Vol. 86, pp. 3808–3812, May 1989
Medical Sciences

Modeling sickle cell vasoocclusion in the rat leg: Quantification of trapped sickle cells and correlation with ^{31}P metabolic and ^{1}H magnetic resonance imaging changes

(sickle cell anemia/erythrocyte/animal model/technetium-99m imaging)

M. E. FABRY*†, V. RAJANAYAGAM*, E. FINE‡, S. HOLLAND§, J. C. GORE§, R. L. NAGEL*, AND D. K. KAUL*

Departments of *Medicine, Division of Hematology, and ‡Nuclear Medicine, Albert Einstein College of Medicine and Montefiore Medical Center, Bronx, NY 10461; and §Department of Diagnostic Radiology, Yale University School of Medicine, New Haven, CT 06510

Communicated by Britton Chance, January 13, 1989

ABSTRACT **We have developed an animal model to elucidate the acute effects of perfusion abnormalities on muscle metabolism induced by different density-defined classes of erythrocytes isolated from sickle cell anemia patients. Technetium-99m (^{99m}Tc)-labeled, saline-washed normal (AA), homozygous sickle (SS), or high-density SS (SS4) erythrocytes were injected into the femoral artery of the rat and quantitative ^{99m}Tc imaging, ^{31}P magnetic resonance spectroscopy by surface coil at 2 teslas, and ^{1}H magnetic resonance imaging at 0.15 tesla were performed. Between 5 and 25 μl of SS4 cells was trapped in the microcirculation of the thigh (or 1–6 × 10^7 cells per cubic centimeter of tissue). In contrast, fewer SS discocytes (SS2) or AA cells were trapped (an equivalent packed cell volume of less than 6.7 μl and 0.3 μl, respectively). After injection of SS4 cells an initial increase in inorganic phosphate was observed in the region of the thigh served by the femoral artery, intracellular pH decreased, and subsequently the proton relaxation time T_1 reached a broad maximum at 18–28 hr. When T_1 obtained at this time was plotted against the volume of cells trapped, an increase of T_1 over the control value of 411 ± 48 msec was found that was proportional to the number of cells trapped. We conclude that the densest SS cells are most effective at producing vasoocclusion. The extent of the change detected by ^{1}H magnetic resonance imaging is dependent on the amount of cells trapped in the microcirculation and the magnitude of the initial increase of inorganic phosphate.**

The pathophysiology of sickle cell painful crisis remains elusive and difficult to study, but the use of magnetic resonance imaging (MRI) and magnetic resonance spectroscopy (MRS) offers a unique insight into the disease process. Sickle cell vasoocclusion is a multistep process (1). The initiation stage is little understood, but irreversibly sickled erythrocytes have been observed obstructing precapillary sphincters (2–5), and such cells have also been shown to be rheologically (6) and hemodynamically incompetent (7). Both clinical and experimental studies suggest that the propagation phase, during which the occlusion is maintained and extended, may involve selective secondary trapping of the densest cells from the patient's blood (8, 9). These cells have the highest intracellular hemoglobin concentration and the greatest rate and extent of polymer formation under deoxy conditions (10, 11). The greater endothelial adhesivity shown by deformable sickle cells may also be involved (12–15). There are no *in vivo* data on the density class most likely to produce vasoocclusion or on the time course of the events involved.

Explanation of vasoocclusion in sickle cell anemia requires that attention be given to the heterogeneity in density and morphology of erythrocytes from patients homozygous for hemoglobin S (SS) (16–19). We have classified and biochemically and rheologically characterized SS red cells in four classes of increasing cell density: SS1, reticulocytes; SS2, discocytes; SS3, very dense discocytes or unsicklable SS discocytes (USDs); and SS4, denser USDs and irreversibly sickled erythrocytes (7, 19).

Painful crises, which are vasoocclusive events, are difficult to diagnose, treat, and study because there are few objective signs capable of verifying occurrence or estimating duration or severity. The disappearance of the densest sickle cells and changes in correlated parameters (8, 20) are objective criteria but do not provide an ongoing picture of the extent and evolution of the infarcted region. Due to its noninvasive character, MRI is a promising modality for the evaluation of vasoocclusion involving muscle or bone marrow. Although there have been reports of MRI-detectable changes in painful crisis (20, 21), the sensitivity of MRI to sickle-cell-induced vasoocclusion of skeletal muscle has not been conclusively demonstrated.

We have developed a model to study the acute effects of sickle-cell-induced vasoocclusion: that is, a single occlusive episode and its sequelae. In this context, a painful crisis in a human might be regarded as multiple occlusive events, as dense cells continue to be removed from the peripheral circulation (8). In the model, the saline-washed, technetium-99m (^{99m}Tc)-labeled dense cell fraction from SS patients is injected into the femoral artery of a rat. The number of cells trapped in the microcirculation is quantified with ^{99m}Tc imaging, changes in the phosphate metabolism of the thigh skeletal muscle (which are indicative of ischemia) are observed by ^{31}P MRS, ^{1}H MRI is used to delineate the affected area, and the extent of tissue damage is assessed by measuring the proton relaxation times T_1 and T_2. Some of the characteristics of painful crisis in the human, such as secondary trapping of dense cells in regions that already contain dense cells, are observed in this model (22).

The objective of the studies reported here was to characterize acute vasoocclusive events and their sequelae—specifically, those attributable to blockage of the microcirculation by dense cells. We will correlate the number of

Abbreviations: MRI, magnetic resonance imaging; MRS, magnetic resonance spectroscopy; T_1 and T_2, proton relaxation times; PCr, phosphocreatine; AA, homozygous for hemoglobin A; SS, homozygous for hemoglobin S.

†To whom reprint requests should be addressed at: Albert Einstein College of Medicine, Department of Medicine, Ullmann Room 921, 1300 Morris Park Avenue, Bronx, NY 10461.

The publication costs of this article were defrayed in part by page charge payment. This article must therefore be hereby marked "*advertisement*" in accordance with 18 U.S.C. §1734 solely to indicate this fact.

density-defined sickle cells trapped in the microcirculation of the rat thigh, the change in phosphate metabolites and intracellular pH, and the magnitude of the MRI-detectable changes in ^1H T_1 and T_2. Preliminary reports of parts of this work have been presented (¶, 23).

METHODS

Preparation of Dense Erythrocytes. Blood from SS patients followed in the Heredity Clinic of the Albert Einstein College of Medicine was obtained after informed consent and characterized by two electrophoretic methods and a solubility test as SS. Dense sickle cells were isolated from freshly drawn, heparinized blood by use of a Percoll–Stractan isopycnic centrifugation technique developed in this laboratory (19, 24). Prior to density fractionation, the whole blood was passed through a Pall filter (Pall Biomedicals) to remove microclots and partially deplete leukocytes; the density separation step completed the removal of all human leukocytes. Erythrocytes were washed three times in sterile, nonpyrogenic saline (NEN), oxygenated with room air, and adjusted to a hematocrit of 30.

Animal Preparation. Female Wistar rats (200–225 g) were anesthetized with pentobarbital (35 mg/kg). A 1.5-cm incision was made in the femoral triangle, and the artery was exposed by blunt dissection and dilated by topical application of 5% hexylcaine hydrochloride (Cyclaine; Merck Sharp & Dohme). Blood flow was temporarily stopped with a hemostatic clip and 0.05–0.5 ml of an erythrocyte suspension (hematocrit, 30) was injected into the femoral artery via a 30-gauge needle. Fifty animals were imaged at 0.15 tesla (T); 46 were observed by ^{99m}Tc imaging; 36 were observed by both ^{99m}Tc imaging and ^1H MRI; data from these 36 animals are presented in Fig. 4.

^{99m}Tc Imaging. Cells were labeled with ^{99m}Tc by using the method of Bardy (25) and a Mallinckrodt pyrophosphate kit (Mallinckrodt Diagnostic Products). The percent free ^{99m}Tc was <5% for AA cells (homozygous for hemoglobin A) and 5–15% for SS4 cells. Animals were imaged by γ camera at 1–2 hr postinjection when ^{31}P MRS was performed or at 2–4 hr when ^1H MRI was performed. γ-Camera imaging was performed using a large-field-of-view Anger camera, peaked for the 140-keV photon of ^{99m}Tc with a 20% window and a high-resolution collimator. Static images were collected with a PDP 11/34 dedicated minicomputer, which allowed the activity of ^{99m}Tc in selected areas to be determined. The equivalent volume of packed cells retained was evaluated by comparing the activity in the area of interest to that in a standardized suspension of the cells used for injection. Appropriate (small) background corrections were made.

NMR Measurements. ^{31}P spectra at 2 T were obtained from intact animals with a 1.5-cm surface coil placed over the thigh muscle, using a General Electric CSI (chemical shift imaging) small-animal spectrometer. A pulse width of 22 μsec was used, giving most of the sample a pulse of 30–60°. A sweep width of 2 kHz, 512 free induction decays, 4000-word blocks, a line broadening of 5 Hz, and a repetition interval of 1.5 sec were used; increasing the repetition interval to 5 sec did not change the ratio of peak heights. Peak areas were evaluated with the GEMCAP program (General Electric) for spectral analysis.

^1H images were obtained at 0.15 T with a resistive prototype imaging system developed in the Department of Diagnostic Radiology at Yale University. A two-dimensional Fourier single-slice imaging technique was used to obtain coronal images from 8-mm slices at 128 × 128 resolution. All 180° pulses were nonselective, and repetition rates of 120, 170, 270, 470, 670, 1070, and 1570 msec were used with an echo time of 15 msec to obtain T_1 data by saturation recovery. T_1 was calculated by fitting an exponential to the intensities from selected regions of interest. For T_2 determinations, a multiecho Carr–Purcell sequence with eight echoes at 20-msec intervals and a repetition rate of 1500 msec was used in combination with the imaging sequence to generate 8-mm axial slices. This sequence employs balanced dephasing gradient pulses before and after each 180° pulse to remove artifactual ("ghost") components of transverse magnetization (26).

Statgraphics version 2.6 (Statistical Graphics, Rockville, MD) was used for statistical analysis.

RESULTS

^{99m}Tc Imaging. Imaging of the intact animal after injection of ^{99m}Tc-labeled erythrocytes demonstrated that 85–100% of the activity was found in three locations. (*i*) In the thigh served by the injected femoral artery, SS4 cells were strongly retained, averaging 16.7 ± 6.9 μl (10–16% of injected cells). There appears to be a saturating volume (20–25 μl) of SS4 cells that can be retained in the thigh (Figs. 1 and 2). Between 0.2% and 2% of the SS4 cells were found in the control leg. SS2 cells were minimally retained, averaging 4.4 ± 2.4 μl. Few AA cells were retained, <0.54 ± 0.2 μl. (*ii*) The reticuloendothelial system of the liver, spleen, and kidneys rapidly trapped cells (60–80% of those injected) that escaped the microcirculation of the thigh. (*iii*) The bladder had significant activity, which originated from (*a*) free ^{99m}Tc present in the injected cell suspension, (*b*) ^{99m}Tc eluted from the cells [≈11% elution was noted for dog red cells at 4 hr (27)], (*c*) free ^{99m}Tc due to catabolism of red cells by the liver or (*d*) ^{99m}Tc bound to hemoglobin released by hemolysis of labeled cells. In labeled cells, 97% of the ^{99m}Tc is attached to the heme or globin (27). The average activity in the bladder (normalized to the total activity) for SS4 cells 1–2 hr after injection was 8.5 ± 4.6% (n = 9) and by 2–4 hr had increased

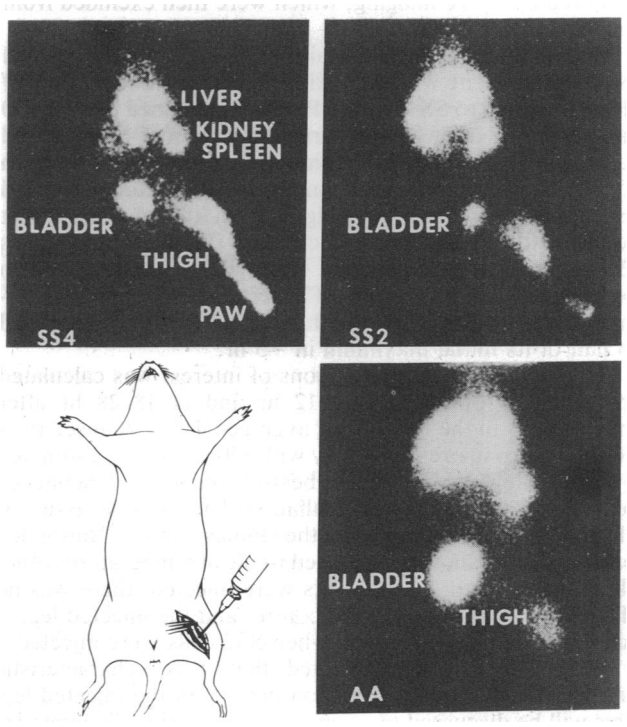

FIG. 1. γ-Camera images of ^{99m}Tc-labeled human AA, SS2, and SS4 erythrocytes injected into the rat femoral artery.

¶Fabry, M. E., Rajanayagam, V., Fine, E., Holland, S., Gore, J. C., Nagel, R. L. & Kaul, D. K., Seventh Annual Meeting of the Society of Magnetic Resonance in Medicine, August 20–26, 1988, San Francisco, p. 632.

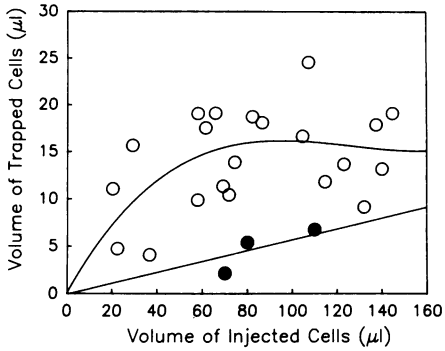

FIG. 2. Equivalent volume of packed red cells retained in the rat thigh versus equivalent volume of packed cells injected for SS4 (○) and SS2 (●). Although the curves were calculated by using a nonlinear regression algorithm, they are merely intended to emphasize the difference in behavior between SS2 and SS4 cells.

to 16.6 ± 4.6% (n = 39). For AA cells the average activity in the bladder at 2–4 hr was 17.3 ± 5.1% (n = 5). Since the animal remains anesthetized between injection and ^{99m}Tc imaging, urination does not complicate the picture. Visible spectroscopy of aspirated urine did not reveal absorption at the Soret wavelength (410–440 nm), which would have indicated the presence of heme or hemoglobin dimers. These results suggest that 75–90% of the activity found in the bladder comes from the first three sources (free ^{99m}Tc) and that very little intravascular hemolysis occurs.

The activity in blood samples obtained after injection was consistent with a half-life of 7 ± 4 min for ^{99m}Tc-labeled human erythrocytes in the rat circulation; therefore, the events described are acute occlusive events.

A source of concern in the interpretation of ^{99m}Tc experiments is the possibility of leakage of labeled cells at the injection site. When AA cells were injected (where little trapping was observed), infrequent site contamination by extravasation was seen. The absence of MRI-detectable changes in 5 SS4-injected animals with "hot spots" confirmed the suspicion of extravasation in 5 of 46 animals observed by ^{99m}Tc imaging, which were then excluded from analysis.

^{31}P MRS. ^{31}P spectra obtained by surface coil yielded results consistent with hypoxia induced by obstruction of blood flow due to SS4 cells. ^{31}P spectra obtained between 30 min and 12 hr after femoral artery injection of SS4 showed varying degrees of inorganic phosphate (P_i) accumulation. In some cases relatively large amounts of P_i accumulated and tissue pH decreased, as judged from the chemical shift between the P_i and phosphocreatine (PCr) spectral peaks (28); 9 hr later P_i levels and tissue pH were returning to normal (Fig. 3). The results of several representative experiments are presented in Table 1. Accumulated P_i was reduced to half of its initial maximum in ≈5 hr.

^{1}H MRI. T_1 in selected regions of interest was calculated from images obtained at 3–12 hr and at 18–28 hr after injection. T_1 in the control leg averaged 411 ± 48 msec (n = 56), which compares favorably with 350 ± 50 msec estimated by Bottomley *et al.* (29) from best-fit frequency dependence of T_1 for a variety of mammalian skeletal muscle tissue. It should be noted that many of the studies cited by Bottomley *et al.* were conducted on excised tissue at temperatures other than 37°C. When AA red cells were injected, there was no difference in T_1 between the control and the injected leg. A similar result was observed when SS2 cells were injected.

When SS4 cells were injected, there was a characteristic increase in the apparent proton density in the injected leg; this will be discussed in a separate manuscript. To minimize animal-to-animal variation of T_1, all results were normalized by dividing the T_1 in the injected leg by the T_1 in the control

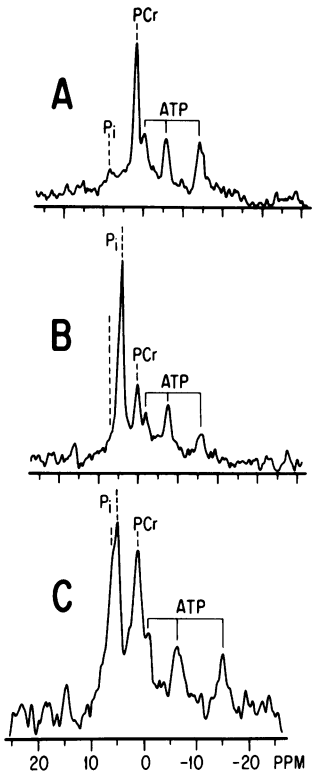

FIG. 3. ^{31}P NMR spectra obtained by surface coil at 35 MHz. (*A*) Control leg. (*B* and *C*) Injected leg (same rat) 4 and 9 hr, respectively, after injection of SS4 cells. Note the shift in P_i in *B* due to reduced pH, and the presence of two partially resolved resonances for P_i in *C* due to some tissue in which the pH had returned to normal.

leg of the same animal: $T_{1(inc)} = T_{1(inj)}/T_{1(cont)}$. When this value was plotted against the volume of cells retained, there was no increase in $T_{1(inc)}$ until >8 μl of cells was retained in the thigh (Fig. 4). A regression of $T_{1(inc)}$ versus the equivalent volume of packed cells retained for SS4 cells only revealed an intercept of 8 μl and a coefficient of determination (r^2) of 56.7% with $P < 0.005$. When very small amounts of SS4 cells were injected and small amounts of cells were retained, no change in $T_{1(inc)}$ was observed. Alternate approaches to the analysis of these data are possible. Since most injections of SS4 resulted in retention of >8 μl of cells, it is reasonable to compare $T_{1(inj)}$ for all animals with less than or more than 8 μl of retained cells. For <8 μl of cells $T_{1(inj)}$ is not statistically different from $T_{1(cont)}$, whereas for >8 μl of cells, $T_{1(inj)}$ (615 ± 42 msec) differs from $T_{1(cont)}$ (411 ± 48 msec) with $P <$ 0.00002. A linear regression line can also be drawn through

Table 1. Relation between early increase of the P_i/PCr ratio and subsequent increase of T_i

Cell type	Volume, μl		Injected/control ratio‡		
	Injected*	Trapped†	P_i/PCr at 3–4 hr	P_i/PCr at 9–12 hr	T_1 at 9–12 hr
SS2	80	5.4	0.94	—	1.006
SS4	90	16.2	1.01	—	1.012
	100	15.8	1.57	1.54	1.058
	90	14.8	1.66	2.59	1.319
	70	23.9	8.73	—	1.625
	90	11.1	9.33	5.37	1.461
	70	24.1	9.92	4.27	1.379

Data are from representative animals.
*Volume of cells injected into animal.
†Volume of cells trapped in injected thigh, determined by ^{99m}Tc imaging 1–2 hr after injection.
‡Ratio for injected leg versus control leg.

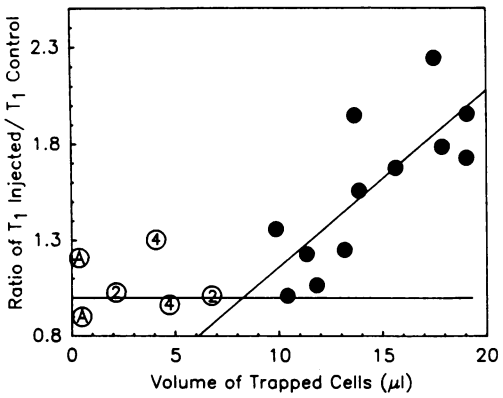

FIG. 4. $T_{1(inj)}/T_{1(cont)}$, measured at the time of maximum change in T_1 and T_2, versus the equivalent packed cell volume for SS4 cells (●), unfractionated AA cells (Ⓐ), SS2 cells (②), or very low doses of SS4 cells (④). The line through the filled circles is a linear regression with $r^2 = 56.7\%$, $P < 0.005$, and an intercept of 8 μl, while that through the open circles merely indicates a ratio of 1.0.

all of the $T_{1(inc)}$ values with an r^2 similar to that of the line drawn only through the SS4 values, which is compatible with the absence of a threshold.

When ^{1}H MRI was performed 3–4 hr after injection of SS4 either no or very small changes in T_1 were observed; however, by 9–12 hr after injection, T_1 values in excess of 500 msec were observed. At 48 hours postinjection T_1 and T_2 were lengthened, but to a lesser extent than was observed in the same animals at 24 hr.

T_2 was measured by a multiecho imaging sequence, taking particular care to ensure that the 180° pulses were appropriately set (26). T_2 for the control leg was found to be 37.5 ± 6.4 msec (n = 20), which compares favorably with the literature value of 40 msec for mammalian skeletal muscle (29). T_2 values for the injected leg exhibited greater variation than T_1 values; the increased variation may stem in part from the use of axial slices for T_2 images, which average T_2 along muscle bundles (which would be more likely to share a common blood supply) in contrast to the use of coronal slices for T_1 images, which average T_1 across muscle bundles. A linear regression of $T_{2(inj)}/T_{2(cont)}$ versus $T_{1(inj)}/T_{1(cont)}$ yielded an r^2 of 58.8%, $P > 0.0005$ (n = 16), and a slope of 1.1, which implies that the relative increase in T_2 is about the same as the relative increase in T_1.

Observation of elevated T_1 in the injected leg 9–12 hr postinjection was highly correlated with early observation of elevated values in the P_i/PCr ratio (Table 1). When P_i/PCr was >5, $T_{1(inj)}/T_{1(cont)}$ averaged 1.49 ± 0.12, whereas when P_i/PCr was <5, $T_{1(inj)}/T_{1(cont)}$ averaged 1.10 ± 0.14; this difference was significant at $P < 0.01$.

The femoral artery was ligated in three animals. At 18–28 hr, $T_{1(inj)}/T_{1(cont)}$ was 0.994 ± 0.058.

Vials of $NiCl_2$ were imaged simultaneously with the animals. T_1 values of 741 ± 77 and 363 ± 24 msec were obtained in 16 separate sessions for 2.5 and 5.0 mM solutions, respectively. This confirms our previous observations of reproducibility on the same system.

DISCUSSION

Vasoocclusion is the primary mechanism of pathological damage in sickle cell disease and is the end product of a complex series of events that involves time-dependent changes not only in the red cell (hemoglobin S polymerization, shape changes, and potassium and water loss) but also in its interaction with the changing microcirculatory environment (changes in vessel tone and perfusion pressure). These arguments justify the need for an *in vivo* experimental system in which the relative importance of these different factors in causing and sustaining occlusion can be evaluated. The intact rat model used in the studies reported here provides such a system. The capillary size and branching structure in the rat microcirculation is similar to that of the human (30).

The experiments described here permit us to draw the following conclusions.

The Densest Cells Are Most Likely to Cause Vasoocclusion. Quantitative ^{99m}Tc imaging demonstrates that AA cells are very weakly retained in the microcirculation of the rat leg. In contrast, sickle cell discocytes (SS2, cells of normal density and rheological properties) are retained to a greater extent and the isolated dense cell fraction (SS4) is very extensively retained (Figs. 1 and 2, Table 1). This quantitative result is in agreement with our previously reported qualitative results (‖, 23). Red cells not retained in the thigh are taken up by the liver, spleen, or kidneys in the reticuloendothelial system. In rat liver, Kupfer cells have been shown to selectively remove human red cells and red cell membranes but not hemoglobin (31). Intravascular hemolysis appears to be minimal in this system.

These experiments demonstrate that sickle cells are less competent in the microcirculation than normal (AA) cells and that SS4 cells are the most likely to be trapped in an *in vivo* model. This is in agreement with the observation that SS4 cells are selectively trapped in *ex vivo* microcirculatory preparations (9) and that they selectively disappear from the peripheral circulation of sickle cell patients during the course of sickle cell painful crisis (8). Further, Kaul *et al.* (15, 32) found that the most adherent cells in the microcirculation are SS2 cells but that blocked postcapillary venules are predominantly filled with SS4 cells that may have been trapped in those vessels narrowed by adhered cells. We may therefore conclude that the densest cells play a major role in propagating and sustaining sickle cell vasoocclusion. The observation that the percent dense cells in a patient's peripheral circulation does not predict the incidence of painful crisis (33) indicates either that the initiation of vasoocclusion involves only a very small number of nondeformable cells or that other mechanisms play a role.

High Energy Phosphates Are Depleted During Vascoocclusion. ^{31}P spectroscopy has been used to determine both metabolite concentration and intracellular pH in living tissue (28). Due to its low pK_a, PCr has a constant chemical shift in the physiological pH range and can serve as an internal reference for the pH-dependent chemical shift of P_i.

Injection of SS4 cells resulted in a larger increase in the P_i/PCr ratio than injection of AA or SS2 cells (Table 1). In addition, the increased P_i was accompanied by changes in the P_i chemical shift that indicated reduced intracellular pH in the skeletal tissue in the sensitive region of the surface coil (28). Red cell 2,3-bis(phospho)glycerate is not detectable at this sensitivity due to the small blood volume in skeletal tissue. The changes observed in P_i and pH are compatible with decreased tissue oxygenation secondary to vasoocclusion. The recovery of normal P_i/PCr ratios with a half-life of 5 hr indicates that occlusion under these conditions is temporary.

T_1 Increases in Proportion to the Number of Cells Retained. In a magnetic resonance image, contrast (or image intensity) is primarily determined by three factors: (*i*) proton density, the number of protons per cubic centimeter of tissue and (*ii* and *iii*) the proton relaxation times (T_1 and T_2), which are the reciprocals of the rates at which magnetization returns to its equilibrium value. In skeletal muscle, water relaxation rates are primarily influenced by water interaction with the hydration layer of cytoplasmic proteins and the hydrated surfaces

‖Fabry, M. E., Kaul, D. K., Lee, H. B., Gore, J. C. & Nagel, R. L., Fourth Annual Meeting of the Society of Magnetic Resonance in Medicine, August 19–23, 1985, London, pp. 1145–1146.

of cellular structures. As water content increases, these interactions are diluted and become less effective and the relaxation times T_1 and T_2 become longer.

Injection of AA or SS2 cell suspensions under oxygenated conditions resulted in no change in T_1 or T_2 of skeletal muscle after 24 or 48 hr. Less than 8 μl of these cells was retained in the microcirculation served by the femoral artery. When the number of cells retained exceeded 8 μl (or 10^7 cells per cubic centimeter of tissue), as occurred when SS4 cells were injected, both T_1 (Fig. 4) and T_2 became longer and reached a maximum at 18–28 hr. This effect is analogous to that observed by others in the case of ischemia (29, 34) and edema (35). Images obtained 48 hr after injection of dense cells suggest that the most intense changes occur between 12 and 36 hr after femoral artery injection.

Even though injection of SS2 cells into the femoral artery results in 10 times more cells trapped than injection of an equivalent volume of AA cells, there is still no increase in T_1 or T_2. Either SS2 cells produce minimal blockage or collateral circulation provides adequate oxygenation to avoid tissue damage. As more SS4 cells are trapped damage occurs. The effects observed here, which are due to blockage of the microcirculation, differ significantly from the effects of femoral artery ligation observed by Challiss *et al.* (36) and in our own experiments. Challiss *et al.* found that ligation produced no change in the perfusion of the resting muscle 12 hr after ligation. We found that ligation of the femoral artery had no effect on tissue T_1 or T_2 18–28 hr after ligation. In both cases the explanation is the presence of an effective collateral circulation that can sustain perfusion. In contrast, extensive blockage of the microcirculation cannot be relieved by collateral circulation.

The results reported here cannot be attributed to either paramagnetic or magnetic susceptibility effects of the heme iron in the trapped cells, for two reasons: (*i*) The number of cells trapped and their distribution are such that their effects on T_1 and T_2 would be negligible and (*ii*) both effects would result in decreased T_2 and/or T_1 rather than the increased T_1 and T_2 observed.

Increased T_1 is accompanied by an equal increase in T_2; this implies that in a clinical setting these events may be detectable by a T_2-weighted pulse sequence.

Early Increase of the P_i/PCr Ratio Correlates with Increased T_1. Increased T_1 in the injected leg does not occur in the absence of an early increase of P_i/PCr (Table 1). This result strongly suggests that the changes detected by ^{1}H MRI are correlated with the extent of the initial vasoocclusion and anoxia.

Summary. We conclude that dense sickle cells are the most likely class of erythrocytes to occlude the microcirculation, that vasoocclusion is followed by early phosphate metabolic changes, and that ^{1}H MRI changes follow later and are dependent on the amount of sickle cells trapped in the microcirculation and the degree of initial phosphate metabolic change. Phosphorus metabolism returns to normal with a half-life of about 5 hr. T_1 increases after 9 hr, reaches a maximum at 18–28 hr, and begins to diminish at 48 hr. Increased T_1 is highly correlated with increased T_2, and T_2-weighted images may detect the effects of sickle cell vasoocclusion.

The technical assistance of Symra Cohen, Wendy Kent, Christina Mazzella, Fanya Schonbuch, and Sandra Suzuka is gratefully acknowledged. This work was funded in part by National Institutes of Health Grants HL37212 and HL21016, National Cancer Institute Grant CA40675, and the American Heart Association, New York Affiliate. S.H. was supported by Public Health Service Grant T32 CA09549 awarded by the National Cancer Institute. All small-animal imaging experiments were carried out in the Department of Diagnostic Radiology at Yale University School of Medicine, New Haven, CT.

1. Nagel, R. L., Fabry, M. E., Billett, H. H. & Kaul, D. K. (1987) *Prog. Clin. Biol. Res.* **240,** 361–380.
2. Klug, P. P. & Lessin, L. S. (1984) *Blood Cells* **64,** 559–563.
3. Baez, S., Kaul, D. K. & Nagel, R. L. (1982) *Blood Cells* **8,** 127–137.
4. Lipowsky, H. L., Sheikh, N. U. & Katz, D. M. (1987) *J. Clin. Invest.* **80,** 117–127.
5. Kurantsin-Mills, J., Jacobs, H. M., Klug, P. P. & Lessin, L. S. (1987) *Microvasc. Res.* **34,** 152–167.
6. Clark, M. R., Mohandas, N. & Shohet, S. B. (1980) *J. Clin. Invest.* **65,** 189–196.
7. Kaul, D. K., Fabry, M. E., Windisch, P., Baez, S. & Nagel, R. L. (1983) *J. Clin. Invest.* **72,** 22–31.
8. Fabry, M. E., Benjamin, L., Lawrence, C. & Nagel, R. L. (1984) *Blood* **64,** 559–563.
9. Kaul, D. K., Fabry, M. E. & Nagel, R. L. (1986) *Blood* **68,** 1162–1166.
10. Noguchi, C. T., Torchia, D. A. & Schechter, A. N. (1983) *J. Clin. Invest.* **72,** 846–852.
11. Eaton, W. A. & Hofrichter, J. (1987) *Blood* **70,** 1245–1266.
12. Mohandas, N. & Evans, E. (1985) *J. Clin. Invest.* **76,** 1605–1612.
13. Barabino, G. A., McIntire, L. V., Eskin, S. G., Sears, D. A. & Udden, M. (1987) *Blood* **70,** 152–157.
14. Hebbel, R. P., Yamada, O., Moldow, C. F., Jacob, H. S., White, J. G. & Eaton, J. W. (1980) *J. Clin. Invest.* **65,** 154–160.
15. Kaul, D. K., Fabry, M. E. & Nagel, R. L. (1988) *Clin. Res.* **36,** 412A (abstr.).
16. Herrick, J. B. (1910) *Arch. Intern. Med.* **6,** 517–521.
17. Seakins, M., Gibbs, W. N., Milner, P. F. & Bertles, J. F. (1973) *J. Clin. Invest.* **52,** 422–432.
18. Clark, M. R., Mohandas, N., Caggiano, V. & Shohet, S. B. (1978) *J. Supramol. Struct.* **8,** 521–532.
19. Fabry, M. E. & Nagel, R. L. (1982) *Blood Cells* **8,** 9–15.
20. Mankad, V. N., Williams, J. P., Harpen, M., Longenecker, G., Brogdon, B. & Moore, B. (1987) *Prog. Clin. Biol. Res.* **240,** 337–350.
21. Rao, V. M., Fishman, M., Mitchell, D. G., Steiner, R. M., Ballas, S. K., Axel, L., Dalinka, M. K., Gefter, W. & Kressel, H. Y. (1986) *Radiology* **161,** 211–215.
22. Fabry, M. E., Fine, E., Nagel, R. L., Rajanayagam, V. & Kaul, D. K. (1987) *Blood* **70,** 60 (abstr.).
23. Fabry, M. E., Kaul, D. K., Davis, L., Gore, J. C., Brown, M. & Nagel, R. L. (1987) *Prog. Clin. Biol. Res.* **240,** 297–304.
24. Fabry, M. E., Mears, J. G., Patel, P., Schaefer Rego, K., Carmichael, L. D., Martinez, G. & Nagel, R. L. (1984) *Blood* **64,** 1042–1046.
25. Bardy, A., Fouye, H., Gobin, R., Beydon, J., de Tovar, G., Pannerciere, C. & Hegesippe, M. (1975) *J. Nucl. Med.* **16,** 435.
26. ODonnell, M., Gore, J. C. & Adams, W. J. (1986) *Med. Phys.* **13,** 182–190.
27. Srivastava, S. C. & Chervu, L. R. (1984) *Semin. Nucl. Med.* **14,** 68–82.
28. Gadian, D. G. & Radda, G. K. (1981) *Annu. Rev. Biochem.* **50,** 69–83.
29. Bottomley, P. A., Foster, T. H., Argersinger, R. E. & Pfeifer, L. M. (1984) *Med. Phys.* **11,** 425–448.
30. Keele, C. A., Neil, E. & Joels, N. (1982) *Applied Physiology* (Oxford University, Oxford), p. 81.
31. Vomel, T., Hager, K. & Platt, D. (1988) *Vet. Immunol. Immunopathol.* **18,** 361–368.
32. Kaul, D. K., Fabry, M. E. & Nagel, R. L. (1989) *Proc. Natl. Acad. Sci. USA* **86,** 3356–3360.
33. Billett, H. H., Kim, K., Fabry, M. E. & Nagel, R. L. (1986) *Blood* **68,** 301–303.
34. Ratner, A. V., Okada, R. D., Newell, J. B. & Pohost, G. M. (1985) *Circulation* **71,** 823–828.
35. Herfkens, R. J., Sievers, R., Kaufman, L., Sheldon, P. E., Ortendahl, D. A., Lipton, M. J., Crooks, L. E. & Higgins, C. B. (1983) *Radiology* **147,** 761–764.
36. Challiss, R. A., Hayes, D. J., Petty, R. F. & Radda, G. K. (1986) *Biochem. J.* **236,** 461–467.